Journal of Computational Neuroscience, 4, 57–77 (1997)

Traveling Waves and the Processing of Weakly Tuned Inputs in a Cortical Network Module

RANI BEN-YISHAI
Racah Institute of Physics and Center for Neural Computation, Hebrew University, Jerusalem 91904, Israel

DAVID HANSEL
Centre de Physique Théorique, UPR014-CNRS, Ecole Polytechnique, 91128 Palaiseau, France

HAIM SOMPOLINSKY
Racah Institute of Physics and Center for Neural Computation, Hebrew University, Jerusalem 91904, Israel; and Luscent Technologies-Bell Laboratories, Murray Hill, NJ 07974 USA

Received February 6, 1996; Revised July 12, 1996; Accepted August 2, 1996

Action Editor: J. Rinzel

Abstract. Recent studies have shown that local cortical feedback can have an important effect on the response of neurons in primary visual cortex to the orientation of visual stimuli. In this work, we study the role of the cortical feedback in shaping the spatiotemporal patterns of activity in cortex. Two questions are addressed: one, what are the limitations on the ability of cortical neurons to lock their activity to *rotating* oriented stimuli within a single receptive field? Two, can the local architecture of visual cortex lead to the generation of *spontaneous* traveling pulses of activity? We study these issues analytically by a population-dynamic model of a hypercolumn in visual cortex. The order parameter that describes the macroscopic behavior of the network is the time-dependent *population vector* of the network. We first study the network dynamics under the influence of a weakly tuned input that slowly rotates within the receptive field. We show that if the cortical interactions have strong spatial modulation, the network generates a sharply tuned activity profile that propagates across the hypercolumn in a path that is completely locked to the stimulus rotation. The resultant rotating population vector maintains a constant angular lag relative to the stimulus, the magnitude of which grows with the stimulus rotation frequency. Beyond a critical frequency the population vector does not lock to the stimulus but executes a quasi-periodic motion with an average frequency that is smaller than that of the stimulus. In the second part we consider the stable intrinsic state of the cortex under the influence of *isotropic* stimulation. We show that if the local inhibitory feedback is sufficiently strong, the network does not settle into a stationary state but develops spontaneous traveling pulses of activity. Unlike recent models of wave propagation in cortical networks, the connectivity pattern in our model is spatially symmetric, hence the *direction* of propagation of these waves is arbitrary. The interaction of these waves with an external-oriented stimulus is studied. It is shown that the system can lock to a weakly tuned rotating stimulus if the stimulus frequency is close to the frequency of the intrinsic wave.

Keywords: orientation selectivity, primary visual cortex, population vector

1. Introduction

The role of the local cortical interactions in shaping the response properties of cortical neurons to sensory stimuli has been a matter of debate. According to the classical model of Hubel and Wiesel (1962) (HW) the receptive field (RF) properties of simple cells in primary visual cortex is a reflection of the feedforward afferents from the lateral geniculate nucleus (LGN). In particular, according to the HW model the preferred orientation (PO) of a simple cell originates from the geometrical alignment of the small, circular RFs of the LGN neurons that project to it. Recently, an experiment in ferret has shown a significant correlation between the RF alignment of the LGN afferents to a site and the PO of cortical cells in the same site (Chapman et al., 1991). In some cases, however, the LGN RFs were not aligned; no overlap between the LGN RFs and that of the cortical cells and no correlation between the sharpness of orientation tuning of cortical cells and the sharpness of alignment of the observed LGN RFs have been found. More recent experiments in cat visual cortex have found a high correlation between the subfield organization of the RFs of simple cells and the RFs of LGN X-cells that are "functionally connected" to them (Reid and Alonso, 1995). In addition, recent intracellular recordings showed substantial orientation tuning of the synaptic inputs from the LGN to cells in cat primary visual cortex, generated by drifting gratings (Ferster et al., 1996). On the other hand, the blockage of extracellular inhibition in cortex caused substantial deterioration of the orientation tuning, suggesting that cortical circuitry plays an important role in shaping the relatively sharp orientation tuning in cortex. (Sillito, 1977; Tsumoto et al., 1979; Sillito et al., 1980; Ferster and Koch, 1987; Hata et al., 1988; Nelson et al., 1994). Furthermore, recent intracellular measurements indicate that the direct LGN input to cells in the input layer 4 constitutes only a fraction of the total, orientation-selective excitatory input to these cells (Ahmed et al., 1994; Douglas et al., 1995; Pei et al., 1994), suggesting that massive cortical excitatory feedback in addition to cortical inhibition may be important in shaping orientation selectivity.

Several recent models that are based on plausible assumptions about the local cortical connections have shown that these connections are capable of playing a central role in generating the sharp selectivity of cortical neurons to the orientation of visual stimuli (Wörgötter and Koch, 1991; Ben-Yishai et al., 1995a; Somers et al., 1995; Hansel and Sompolinsky, 1996a; Vidyasagar et al., 1996) and their direction of movement (Suarez et al., 1995; Maex and Orban, 1992). These models focused primarily on the response of cortical neurons to the appearance of a stimulus with a fixed orientation or direction. Responses to time-dependent, time-oriented stimuli have received little attention, both experimentally and theoretically.

In this work we broaden the scope of previous theoretical studies to the spatiotemporal domain. We study how a spatial pattern of activity that is generated by a cooperative mechanism in the cortex interacts with an external input whose features change with time. Specifically, our working hypothesis is that the primary visual cortex encodes the orientation of a local edge by the distributed response profile of the orientation columns whose receptive field is stimulated by the edge. We further assume that the local cortical network receives *weakly tuned input from the LGN* and generates a sharply tuned response due to the combination of massive excitatory feedback and inhibition from within the network (Ben-Yishai et al., 1995a; Somers et al., 1995; Hansel and Sompolinsky, 1996a). The fundamental assumption of this work is that the underlying cortical circuitry is capable of generating sharply tuned responses even for stimuli that generate only weakly tuned inputs to the cortex. Such stimuli can always be constructed by controlling the spatial extent and geometry of a visual stimulus, in such a way that even a substantial alignment of the LGN RFs will generate only weakly tuned inputs to the cortex. It is important to emphasize that this assumption does not rule out the possibility that certain visual stimuli, such as gratings with appropriate spatial frequencies, generate LGN inputs to the cortical cells that are substantially tuned to the orientation of the stimuli.

These assumptions raise these questions: How does the population activity profile evolve in time in the presence of a rotating stimulus? Does it lock to the stimulus motion in frequency only or also in phase? For what range of rotation frequencies does this locking occur?

Another issue addressed in this article is the appearance of traveling pulses of activity in neuronal networks. In recent years, traveling bursts of activity have been observed in cortex (Gutnick et al., 1982; Chagnac-Amitai and Connors, 1989; Wadman and Gutnick, 1993), superior colliculus (Munoz et al., 1991), thalamus (Kim et al., 1995) and hippocampus (Miles et al., 1988; Traub et al., 1993). Spatiotemporal oscillations of neuronal activity in olfactory systems have been extensively studied (Freeman, 1975; Laurent and Naraghi, 1994; Kleinfeld et al., 1994; Li and Hopfield, 1989). Neither the mechanisms that

generate these waves nor their functional relevance are well understood. Several models have investigated internal cooperative mechanisms for the spontaneous generation of traveling waves in neuronal networks (Idiart and Abbott, 1993; Ermentrout and McLeod, 1993; Golomb et al., 1996). In addition, moving pulses of activity have been implicated in the coding of motor trajectories. Examples are the Moving Hill hypothesis regarding the control of eye movement in the superior colliculus (Guitton, 1992), and the time-dependent population vector hypothesis regarding the coding of arm movement in motor cortex (Georgopoulos et al., 1988; Georgopoulos, 1995; Schwartz, 1993; Lukashin et al., 1995). Here we study the appearance of traveling waves in the context of a neuronal network that codes for an angle. We show that a cortical hypercolumn, activated by an isotropic input, can exhibit a stable spatiotemporal pattern consisting of a profile of activity that moves across the different orientation columns. We then study the interaction of this intrinsic wave with a rotating external input.

The architecture and dynamics of our model is presented in Section 2. In Section 3 we study the stationary states of the system. The response to a time-dependent (rotating) input is investigated in Section 4. In Section 5 we study parameter regimes where the intrinsic stable states consist of traveling waves. The properties of these waves and their response to a rotating input is studied. In Section 6 we discuss our results and their functional consequences.

2. The Model

We consider a simplified neural network model of a single hypercolumn in the primary visual cortex. The network consists of N_E excitatory neurons and N_I inhibitory neurons that code for the orientation of a visual stimulus appearing in a common visual field. The neurons are parametrized by an angle θ, distributed uniformly between $-\pi/2$ and $+\pi/2$, that denotes their preferred orientation (PO). We assume periodic boundary conditions – that is, neurons with PO $-\pi/2$ and $+\pi/2$ are the same. The interaction between a presynaptic excitatory neuron θ' and a postsynaptic neuron of type L, θ, is denoted by $\frac{1}{N_E} J_{LE}(|\theta - \theta'|)$. The index $L = E, I$ denotes the two populations of excitatory and inhibitory neurons. The interaction between a presynaptic inhibitory neuron θ' and a postsynaptic neuron of type L, θ, is denoted by $\frac{1}{N_I} J_{LI}(|\theta - \theta'|)$. The functions J_{LK} represent the dependence of the interaction between neurons on the similarity of their POs; the interaction is strongest in amplitude for neurons that belong to the same orientation column. These functions are periodic, with period π. The network architecture is shown in Fig. 1.

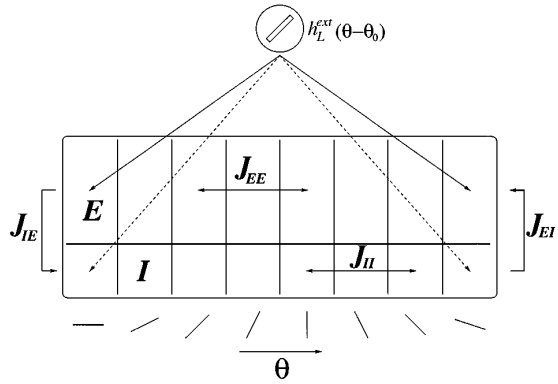

Figure 1. The network consists of excitatory (E) and inhibitory (I) neurons in a single hypercolumn in the primary visual cortex. The neurons are parameterized by an angle θ, which denotes their preferred orientation. All neurons receive external input, which represents a visual stimulus with orientation θ_0 appearing in a common visual field. The connectivity in the network is full. The interactions within and between the different populations are defined in the text.

We study population dynamic equations, which describe the temporal evolution of the activity of the different orientation columns. The activity of the column θ at time t is represented by two continuous functions, $m_E(\theta, t)$ and $m_I(\theta, t)$, $0 \le m_E, m_I \le 1$. These functions represent the activity of the excitatory and inhibitory neurons with POs in the neighborhood of θ, at time t, relative to the saturation activity level. We refer to m_E and m_I, respectively, as the excitatory and inhibitory activity profiles of the system. They obey the following dynamic equations (Ben-Yishai et al., 1995a; Wilson and Cowan, 1972):

$$\tau_0 \frac{d}{dt} m_L(\theta, t) = -m_L(\theta, t) + g(h_L(\theta, t)) \quad L = E, I, \tag{1}$$

where τ_0 is a microscopic characteristic time assumed to be of the order of a few milliseconds. The quantities $h_L(\theta, t)$ are the total synaptic inputs to the neurons of the L-th type in the column θ, relative to their thresholds, T_L. They are given by

$$h_L(\theta, t) = \sum_{K=E,I} \int_{-\pi/2}^{+\pi/2} \frac{d\theta'}{\pi} J_{LK}(\theta - \theta') m_K(\theta', t) + h_L^{\text{ext}}(\theta, t) - T_L. \tag{2}$$

The quantities $h_L^{\text{ext}}(\theta, t)$ represent the inputs from the LGN to the L-th population in the cortical columns. We choose the following functional forms for the cortical interactions

$$\begin{aligned} J_{LE}(\theta) &= J_0^{LE} + J_2^{LE}\cos 2\theta, \qquad J_0^{LE} \geq J_2^{LE} \geq 0 \\ J_{LI}(\theta) &= -J_0^{LI} - J_2^{LI}\cos 2\theta, \qquad J_0^{LI} \geq J_2^{LI} \geq 0. \end{aligned} \tag{3}$$

This choice implies that both excitatory and inhibitory interactions are maximal for neurons with similar POs, in agreement with experiment (see Georgopoulos et al., 1993). Substituting Eqs. (3) in Eq. (2), the synaptic inputs can be written as

$$\begin{aligned} h_L(\theta, t) = &\\ J_0^{LE} m_0^E - J_0^{LI} m_0^I + J_2^{LE} m_2^E \cos\left(2(\theta - \psi_E)\right) &\\ - J_2^{LI} m_2^I \cos\left(2(\theta - \psi_I)\right) + h_L^{\text{ext}}(\theta, t) - T_L, & \end{aligned} \tag{4}$$

where m_0^L, m_2^L, and ψ_L are defined in terms of the following order parameters:

$$m_0^L(t) = \int_{-\pi/2}^{+\pi/2} \frac{d\theta}{\pi} m_L(\theta, t) \tag{5}$$

and

$$\mathbf{P}_L(t) = \int_{-\pi/2}^{+\pi/2} \frac{d\theta}{\pi} m_L(\theta, t) e^{2i\theta} = m_2^L(t) e^{2i\psi_L(t)}. \tag{6}$$

The first-order parameter m_0^L measures the activity of the two types of neurons averaged over the entire network. The second-order parameter $\mathbf{P}_L$ measures the degree of the spatial modulation in the activity profiles. It is a complex number that represents a vector in two-dimensions. This vector is the *population vector* of the system, evaluated by summing unit vectors pointed in the POs of the neurons, weighted by their instantaneous activities (Georgopoulos et al., 1988; Seung and Sompolinsky, 1993). The angle ψ_L denotes the orientation of the population vector and m_2^L denotes its length – that is, the strength of the angular modulation of the population. From a functional point of view it is useful to consider $\psi_E(t)$ as a population coding of the stimulus orientation. By integrating Eq. (1) over θ, with and without a factor $e^{2i\theta}$, one reduces the equations to solving first-order nonlinear differential equations for $m_0^L(t)$ and $\mathbf{P}_L(t)$.

Finally, we use a semilinear gain function – $g(h) = 0$ for $h \leq 0$, $g(h) = h$ for $h \geq 0$, and $g(h) = 1$ for $h \geq 1$. The particular functional forms of the interactions and the gain-function were chosen for the sake of simplicity. More general forms yield a qualitatively similar behavior.

3. Stationary State

We first study the case where the system settles in a stationary state, in the presence of a time-independent stimulus, $h_L^{\text{ext}}(\theta, t) = h_L^{\text{ext}}(\theta)$. The stationary profile is determined by the self-consistent equations

$$m_L(\theta) = g(h_L(\theta)). \tag{7}$$

We model the stimulus by

$$h_L^{\text{ext}}(\theta) = C_L(1 - \epsilon + \epsilon\cos(2(\theta - \theta_0))) \qquad 0 \leq \epsilon \leq 0.5. \tag{8}$$

This choice represents a tuned input originating from a visual stimulus that is oriented at angle θ_0. The parameter C_L denotes the maximal amplitude of the external input from LGN to the Lth population. It thus represents the overall strength of the afferent LGN input. It is assumed to be of the form

$$C_L = C\lambda_L, \tag{9}$$

where C denotes the contrast of the stimulus, and λ_L represents the transfer function from the LGN to the cortex, which may be different for excitatory and inhibitory neurons. The parameter ϵ denotes the angular anisotropy of the LGN input to the cortical hypercolumn (Hubel and Wiesel, 1962; Chapman et al., 1991; Reid and Alonso, 1995). In the limit $\epsilon = 0.5$ the external input to neurons with PO orthogonal to θ_0 is zero. This corresponds, in our parametrization, to maximally tuned inputs. A more general model of $h_L^{\text{ext}}(\theta)$ will include higher harmonics and thus will be able to incorporate narrower inputs. As stated in the Introduction, we focus here on weakly tuned inputs and hence will assume that $\epsilon \ll 1$. In the limit $\epsilon = 0$ the external input to all neurons in the same population is identical. It is important to note that the value of ϵ is determined both by the geometric features of the visual stimulus, as well as by the geometric organization of the LGN afferents to individual cortical neurons (see Introduction).

3.1. Homogeneous State

The rotational symmetry of the network implies that when $\epsilon = 0$ there is always a homogeneous solution,

$m_L(\theta, t) = m_0^L$, which agrees with the naive expectation that orientation selectivity disappears when the external input is isotropic. In this state, $\mathbf{P}_L$ are zero. The mean activity levels of all the neurons in the two populations respectively can be written as

$$m_L = \chi_L(C_L - T_L). \tag{10}$$

The prefactors χ_L are the linear response coefficients of the system, or simply the gain of the system. They are given by

$$\begin{aligned} \chi_E &= \frac{1 - \kappa\tilde{K}}{(\tilde{K} - \tilde{J}^{-1})J_0^{IE}} \\ \chi_I &= \frac{1 - \kappa^{-1}\tilde{J}}{(\tilde{K}^{-1} - \tilde{J})J_0^{EI}}, \end{aligned} \tag{11}$$

where

$$\kappa = \frac{C_I - T_I}{C_E - T_E} \tag{12}$$

and

$$\tilde{K} = J_0^{EI}/\left(J_0^{II} + 1\right); \quad \tilde{J} = J_0^{IE}/\left(J_0^{EE} - 1\right). \tag{13}$$

Note that the effect of the cortical interactions on the level of activity of the excitatory neurons is twofold. The excitatory feedback J_0^{EE} tends to amplify the response, whereas the inhibitory interaction J_0^{IE} tends to suppress it. Whether the net effect is an enhancement of the activity or the converse depends on the assumed values of these parameters (compare with Douglas et al., 1995).

The above equations are valid of course only for parameters such that $m_L > 0$. Depending on the system parameters, there can be homogeneous states (with nonzero activity) even for subthreshold inputs.

3.2. Inhomogeneous State

3.2.1. Afferent Mechanism. When the input to the cortical network is anisotropic – that is, $\epsilon > 0$ – the activity profile is, of course, nonuniform, and some tuning to orientation will develop. Solving the self-consistent equations for the profile is relatively simple in the case of the semilinear gain function. We will consider here the case of sharp tuning, where for each stimulus orientation a fraction of the populations remains inactive. Such a state, which occurs for a wide range of parameters, has the profile

$$\begin{aligned} m_L(\theta) = H_L\,(\cos 2(\theta - \psi_L) - \cos(2\theta_L)) \\ |\theta - \psi_L| < \theta_L, \end{aligned} \tag{14}$$

and $m_L(\theta) = 0$ otherwise. Equations for the amplitudes, H_L, the tuning widths, θ_L, and the angles, ψ_L, are derived by substituting Eq. (14) in Eqs. (5) and (6), and solving the resultant self-consistent equations. For the population angles they yield

$$\psi_L = \theta_0 \tag{15}$$

as expected. The details are presented in Appendix A.

The sharpness of the tuning depends on the cortical interactions. If their angular modulation is weak relative to the external input, the system mimics the simple Hubel-Wiesel afferent mechanism of orientation selectivity (Hubel and Wiesel, 1962). In this case, to obtain sharp tuning ϵ needs to be large. Alternatively, C has to be small so that the population is always only slightly above the threshold. Examples are shown in Figs. 2A–F, which display the results of numerical integration of the population dynamic equations, Eq. (1). Here and in the rest of the paper the numerical results are obtained using numerical integration with fourth-order Runge-Kutta method and an angular resolution of 1 deg. The results of Figs. 2A–F correspond to the case where the spatial modulation of the excitatory feedback is roughly the same as that of the inhibitory one; hence the net modulated feedback is weak. Consequently, when the input tuning is weak and C is large the tuning is broad, as shown in Figs. 2A, B. Sharp tuning is obtained when C is close to threshold (Figs. 2C, D) or ϵ is large (Figs. 2E, F). Figures 2A, C, and E display the activity profiles m_E and m_I. Figures 2B, D, and F display the relationship between the external inputs (solid and dashed lines) and the cortical feedback. The latter is represented by an effective threshold $T_{\text{eff}}(\theta)$ (dotted line) defined as $T_{\text{eff}} = h_L^{\text{ext}}(\theta) - h_L(\theta)$. Hence, $m_L(\theta) = g(h_L^{\text{ext}}(\theta) - T_{\text{eff}}(\theta))$. Note that for simplicity we have chosen here parameters such that the effective threshold is the same for the excitatory and inhibitory populations.

3.2.2. Marginal Phase. If the spatial modulation of the cortical interactions is strong, sharp tuning may be obtained even for a weakly tuned stimulus. In the extreme case, the homogeneous state is unstable even for $\epsilon = 0$. Instead, the stable solution is an inhomogeneous state with a profile as described above, with an arbitrary location of the peak. This solution represents spontaneous generation of orientation selectivity. Thus, in this regime there is a continuum of possible stable states, all represented by identical activity profiles but with different locations of their peaks.

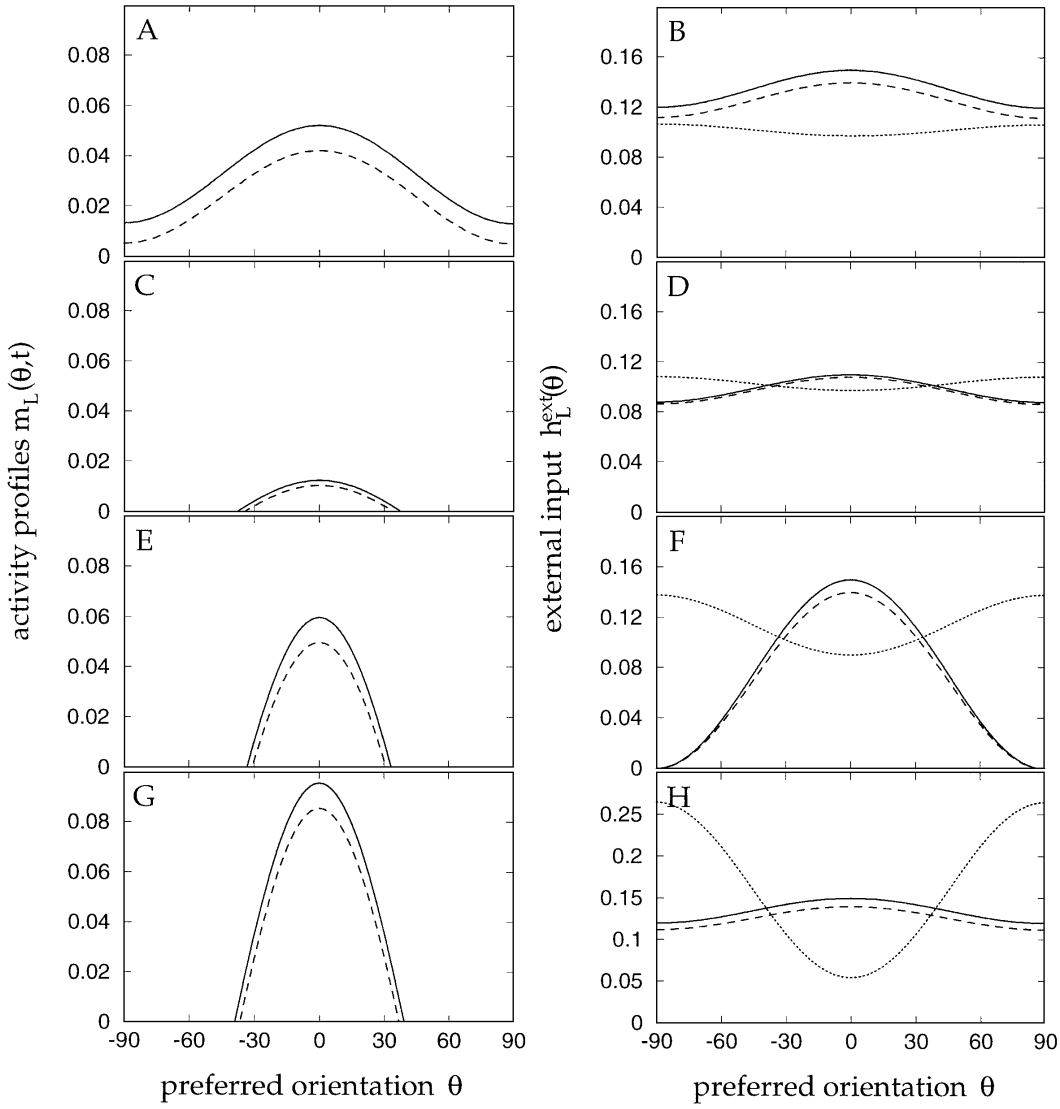

Figure 2. Orientation tuning in the case where the modulation of the cortical interactions is weak, A–F, and in the marginal phase, G–H. A, C, E, G: Solid and dashed lines are the excitatory and inhibitory activity profiles, $m_E(\theta)$ and $m_I(\theta)$, respectively. B, D, F, H: Solid and dashed lines are the inputs to the excitatory and inhibitory populations, $h_E^{\rm ext}(\theta)$ and $h_I^{\rm ext}(\theta)$, respectively. Dotted line is the effective threshold $T_{\rm eff}(\theta)$; A–B: $\epsilon = 0.1$, $C_E = 0.15$ and $C_I = 0.14$. All neurons are active, $\theta_E = \theta_I = 90^\circ$; C–D: $\epsilon = 0.1$, $C_E = 0.11$ and $C_I = 0.108$. Only neurons with θ close to $\theta_0 = 0^\circ$ are above their threshold. Sharp tuning is achieved via small C; E–F: $\epsilon = 0.5$, $C_E = 0.15$ and $C_I = 0.14$. Sharp tuning is achieved via large ϵ. Model parameters for A–F are $T_E = T_I = 0.1$, $J_0^{EE} = J_0^{IE} = 13$, $J_2^{EE} = J_2^{IE} = 9$, $J_0^{EI} = J_0^{II} = 18$, $J_2^{EI} = J_2^{II} = 9$; G–H: $\epsilon = 0.1$, $C_E = 0.15$ and $C_I = 0.14$. Model parameters are as in A–F, except for the modulation of the excitatory interactions, $J_2^{EE} = J_2^{IE} = 12.5$.

This solution is called a marginal phase because there are no barriers between the different fixed points of the dynamics. The overall amplitude of the population response, H_L, in any one of these states, is determined by the input contrast C, but the width of the activity profiles is determined by the cortical interactions. The width depends also on the *relative* inputs to the two populations – namely, κ, Eq. (12) – but this dependence is rather weak.

In reality, the location of the peak of the activity is not arbitrary but is determined by the orientation of the external input. Therefore, in a realistic implementation of

the last scenario, ϵ is assumed to be nonzero but small. Since ϵ is small, the main effect of the anisotropy of the input is to select among the continuum of possible states that state in which the location of the peak in the activity matches the orientation of the stimulus, but it will not have much effect on the width of the activity profile. The equations of the marginal phase are given in Appendix A. Its properties were discussed in detail in Ben-Yishai et al. (1995a). An example of a tuning curve in this regime is shown in Fig. 2G. Here the angular modulation of the excitatory interactions is larger than the inhibitory ones so that the net modulation of the cortical feedback is large and the system is in the marginal phase.

4. Response to Rotating Stimulus

We now consider an external stimulus in the form of a short-oriented object that rotates within a single receptive field. This is modeled by a time-dependent external angle – that is, $\theta_0 = \theta_0(t)$, (see Fig. 3). If the system encodes the instantaneous stimulus orientation by the population vector, then the population activity profile should be able to follow the rotation of the stimulus. This raises the following questions: Can the population activity profile lock to the input? If so, what is the range of input angular velocities for which such locking occurs? For a stimulus that varies on time scales comparable to single-cell time constants, the answers to the above questions may depend strongly on the details of the single-cell microscopic dynamics. However, when the temporal variation of the stimulus is slow, and in addition the direct coupling of the population profile to the rotating stimulus is relatively weak, cortical cooperative effects may be the dominant factor in determining the locking properties. We therefore focus here on the case of a weakly tuned ($\epsilon \ll 1$) and slow time-dependent ($\dot{\theta}_0 = O(\epsilon)$) input.

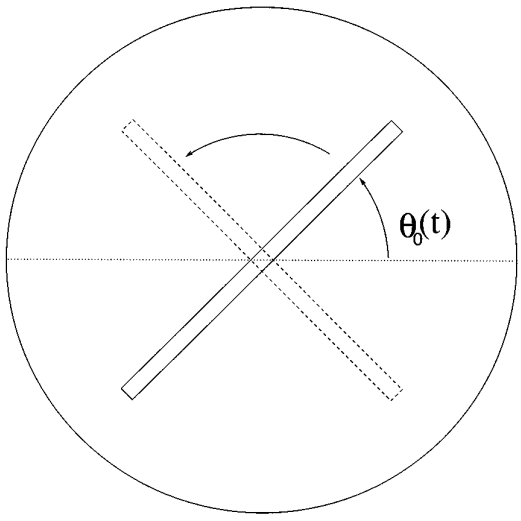

Figure 3. A stimulus with a time-dependent orientation $\theta_0(t)$ is presented in a common receptive field.

We first consider the case where the cortical interactions are such that the orientation tuning is dominated by the input. In this case, when ϵ is small, the spatial modulation of the population profile induced by the input is small and represents essentially the linear response of the system to ϵ. When the stimulus rotates, this linear response is locked to the stimulus with a constant phase shift that is proportional roughly to $\dot{\theta}_0\tau_0$. Thus in this case we expect that the system will lock to the stimulus but that this locking will involve only a small component of the system activity, relative to the DC component. An example is shown in Fig. 4A. As mentioned above, this will be the case up to high stimulus frequencies where the nonlinearity of the single-cell dynamics may prevent complete locking to the stimulus.

The situation is qualitatively different in the parameter regime of the marginal phase. Here the tuning of the network may be sharp, and hence the response to the stimulus is highly nonlinear. Fortunately, in this regime the dynamics can be studied analytically using the approximation of phase dynamics, which becomes exact in the limit of $\epsilon, \dot{\theta}_0 \to 0$. In this limit, the rotation of the stimulus generates a motion of the activity profiles but does not change their shape. Hence the state of the system is given by

$$m_L(\theta, t) = M_L(\theta - \psi_L(t)), \tag{16}$$

where $M_L(\theta)$ are the steady-state activity profiles of the two populations centered at $\theta = 0$ for $\epsilon = 0$. In terms of the order parameters defined above, Eq. (16) means that m_0^L and m_2^L are the same as in the stationary state at $\epsilon = 0$. However, the population angles $\psi_L(t)$, which, as described above, denote the position at time t of the peaks of the profiles of activity, are now time-dependent. The degree of locking to the rotating stimulus is measured by the phase-shifts Δ_L, defined as

$$\Delta_L(t) = \psi_L(t) - \theta_0(t). \tag{17}$$

Because we assume now that the modulation of the input is small and it is only slowly rotating, the rate of change of Δ_L is also small, and in addition the

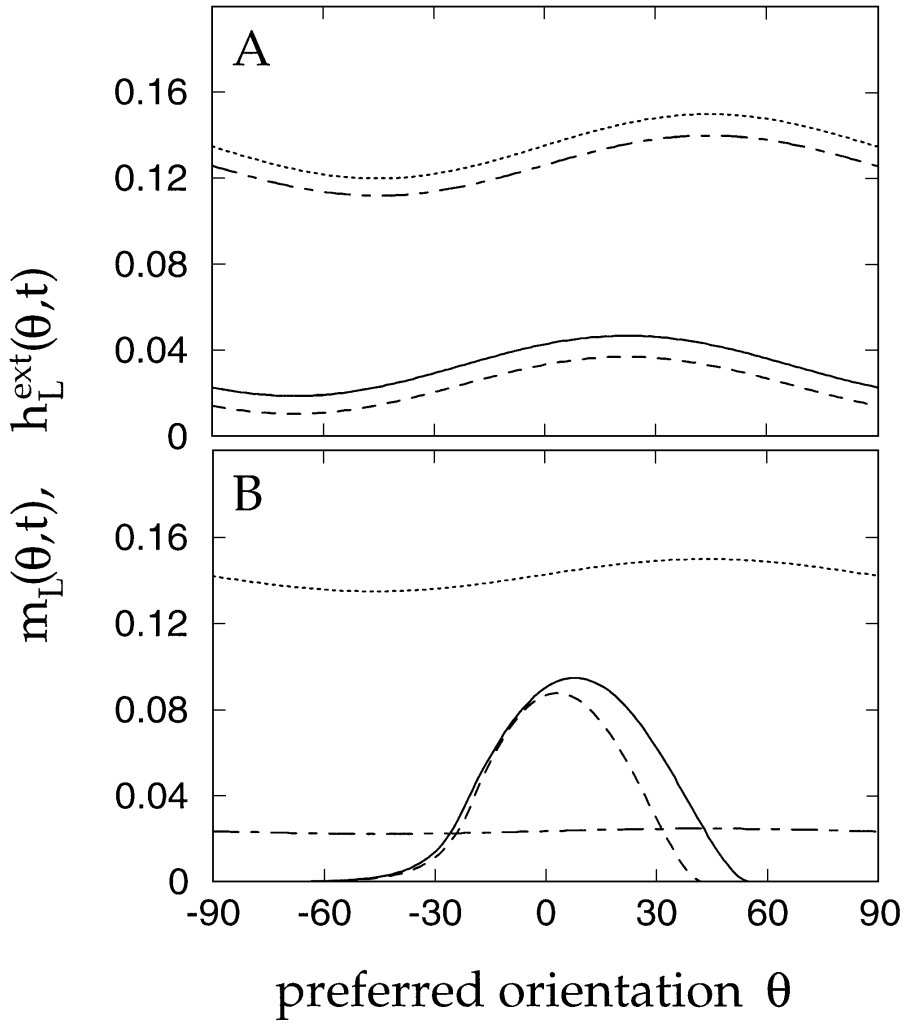

Figure 4. Locking of the activity profiles to a rotating external input in the Hubel-Wiesel mechanism (A) and in the marginal phase (B). Solid and dashed lines are the excitatory and inhibitory activity profiles, $m_E(\theta,t)$ and $m_I(\theta,t)$, respectively. Dotted and dot-dashed lines are the external input to the excitatory and inhibitory populations, $h_E^{\rm ext}(\theta,t)$ and $h_I^{\rm ext}(\theta,t)$, respectively; A: the angular velocity of the stimulus is $\omega = 0.4$ rad$/\tau_0$, where τ_0 is the neuronal time constant, and $\epsilon = 0.1$. The activity profiles have a small component which locks to the stimulus with a constant phase shift of $\sim 20^\circ$. Model parameters as in Fig. 2A; B: $\omega = 0.15$ rad$/\tau_0$ and $\epsilon = 0.05$. Model parameters are: $T_E = T_I = 0.1$, $C_E = 0.15$, $C_I = 0.025$, $\kappa = -1.5$, $J_0^{EE} = J_0^{IE} = 13$, $J_2^{EE} = J_2^{IE} = 12.5$, $J_0^{EI} = 20$, $J_2^{EI} = 9$, $J_0^{II} = 17$, $J_2^{II} = 6$.

difference $\Delta_I - \Delta_E$ is small, $\Delta_I - \Delta_E = O(\epsilon)$, but the phase shifts Δ_L themselves are in general large. The angular velocity of $\Delta \equiv \Delta_E \approx \Delta_I$ is given by the following phase equation (see Appendix C):

$$\frac{d\Delta}{dt} = -\frac{d\theta_0}{dt} + \omega_c \sin(2\Delta), \tag{18}$$

where $\omega_c > 0$ is a characteristic frequency that is proportional to ϵ/τ_0 with a proportionality constant that depends on other system parameters.

The degree of locking of the network population to the external stimulus depends of course on the nature of the time-dependence of θ_0. Below we consider the simple case of a stimulus rotating with a *constant* angular velocity:

$$\frac{d\theta_0}{dt} = \omega. \tag{19}$$

Substituting Eq. (19) in Eq. (18) one observes that for $\omega < \omega_c$, Eq. (18) has a stable fixed point

$$\Delta = \frac{1}{2}\arcsin(\omega/\omega_c). \tag{20}$$

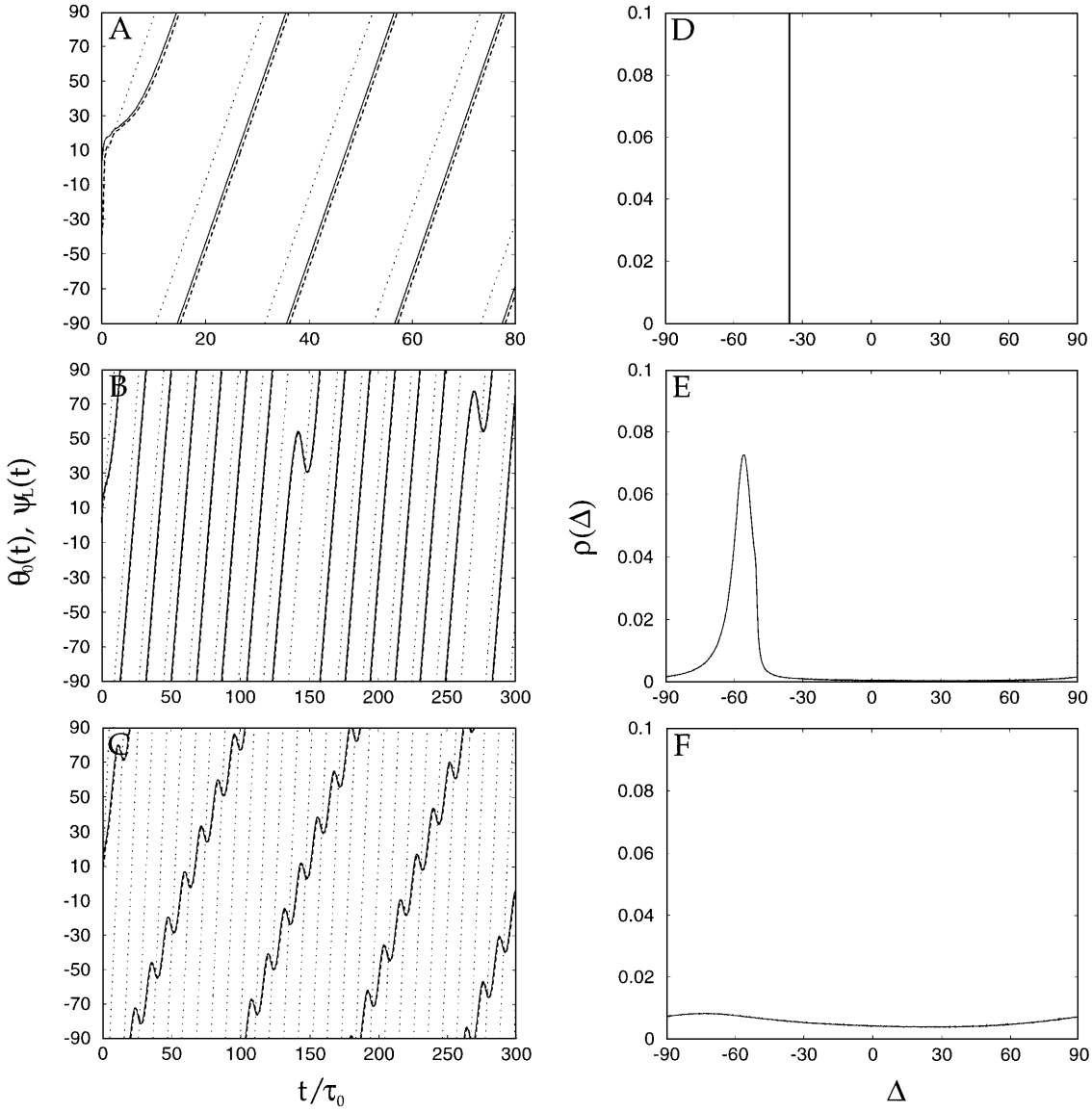

Figure 5. Response to a rotating stimulus in the marginal phase. A–C: Dotted line is the orientation of the visual stimulus, $\theta_0(t) = \omega t$, as a function of time. Solid and dashed lines are the angles of the excitatory population vector, $\psi_E(t)$, and the inhibitory one, $\psi_I(t)$, respectively; A: complete locking of the activity profile to a visual stimulus rotating with frequency $\omega = 0.15$ rad/τ_0. The activity profile follows the stimulus with a constant phase lag; B: partial locking in the case $\omega = 0.175$ rad/τ_0; C: no locking in the case $\omega = 0.3$ rad/τ_0. D–F: The distribution of relative phases, $\rho(\Delta)$; D: complete locking—$\rho(\Delta)$ is a delta function; E: partial locking—$\rho(\Delta)$ has a pronounced peak at 55°; F: no locking—$\rho(\Delta)$ is essentially flat. Model parameters (except for ω) are as in Fig. 4B. For these parameter $\omega_c = 0.173$ rad/τ_0.

It corresponds to a state in which the activity profile is locked to the stimulus and follows it with a constant phase lag. For $\omega \to \omega_c$ the phase lag between the excitatory population and the stimulus reaches $\frac{\pi}{4}$. It should be emphasized that here, unlike in the previous case, the locking is strong in that it involves the motion of a sharply tuned population profile, as shown in Fig. 4B. The angles of the population vectors and the stimulus angle in such a case are shown in Fig. 5A. The results of Fig. 5 are obtained by numerical integration of the full population dynamics, Eq. (1), with a rotating input.

For $\omega > \omega_c$ the fixed point of Eq. (18) disappears, hence the activity profile is not frequency locked to the rotating stimulus. In this regime, the solution of the

phase equation yields

$$\Delta(t) = \arctan\left\{\frac{\omega_c}{\omega} + \frac{\Omega}{\omega}\tan(\Omega(t-\tau))\right\}, \qquad (21)$$

where

$$\Omega = \sqrt{\omega^2 - \omega_c^2} \qquad (22)$$

and τ is determined by the initial condition $\Delta(0) = \Delta_0$. The phase Δ is periodic in time with a period $T = \frac{2\pi}{\Omega}$. Thus, the rotation of the population vector is quasi-periodic, with $\psi_L(t) = \omega t - \Delta(t)$. The average frequency of the population vector rotation is $\omega - \Omega$, which is slower than the stimulus frequency, ω. An interesting feature of $\psi_L(t)$ is its nonmonotonicity. Each time it encounters the stimulus, its reverses its sign and executes a small-amplitude oscillation. The frequency of such encounters is Ω. The behavior of $\psi_L(t)$ in this frequency regime is shown in Fig. 5B for a value of ω close to ω_c, and in Fig. 5C for a higher frequency. They are in a good qualitative agreement with the predictions of the above phase equations, which are based on the limit of small ϵ and ω.

The above results imply that for $\omega > \omega_c$ the relative phase between the system and the stimulus is not fixed but depends both on time and on the initial conditions. Nevertheless, it can be seen from Fig. 5B that near ω_c the system spends considerable amount of time in a roughly fixed phase relative to stimulus. Hence there is partial locking to the stimulus. As ω increases, this partial locking weakens and eventually disappears. To quantitatively assess this property it is useful to consider the distribution of relative phases evaluated by averaging $\Delta(t)$ over time. From Eq. (18) it is evident that

$$\rho(\Delta) = \frac{A}{\omega - \omega_c \sin(2\Delta)}, \quad \omega > \omega_c. \qquad (23)$$

Thus, the approximate phase model predicts that the distribution has a peak at $\Delta = \frac{\pi}{4}$, which is narrow near ω_c and broadens as ω increases. Figures 5E and F show the numerically evaluated distribution of Δ for the parameters of Figs. 5B and C. For comparison we present in Fig. 5D the distribution in the locked regime, where it is simply a delta function centered at the fixed point value, Eq. (20). The predicted gradual broadening of the phase distribution as ω increases is evident, although, in contrast to the approximate phase equations,

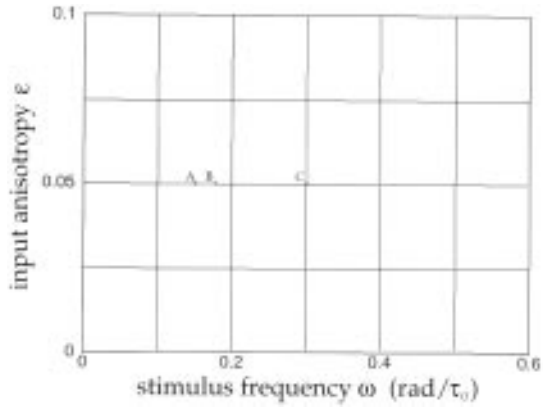

Figure 6. Phase diagram for locking to a rotating stimulus, in the marginal phase. The shaded area is the parameter regime where a phase locked solution is stable. The phase lag between the stimulus orientation and the population vector angle for a given ϵ continuously increases across this area (not shown), and reaches its maximum at $\omega = \omega_c(\epsilon)$. Points A–C indicate values of ω and ϵ used in Figs. 5A–C, respectively. Model parameters are as in Fig. 4B.

the actual peak of the distribution is at angles greater than $\frac{\pi}{4}$.

Figure 6 displays the full phase diagram for locking to a rotating stimulus in the plane of stimulus parameters, ϵ-ω. The border of the shaded area represents $\omega_c(\epsilon)$, which is the transition line from locked to unlocked states. This phase diagram has been evaluated numerically from the full dynamic equations. For small ϵ, $\omega_c(\epsilon)$ is proportional to ϵ, and the evaluated constant phase lags for $\omega < \omega_c$ are in agreement with Eq. (20).

5. Intrinsic Propagation of Activity Profile

5.1. Isotropic Input

So far we have considered parameters where, for a static stimulus, the system reaches a stationary state. Can our network generate an *intrinsic* state of a propagating activity profile? We have found that there are parameter regimes for which the stable solution is a traveling wave of the form of a propagating pulse of neuronal activity, even for $\epsilon = 0$. This solution is of the form

$$m_L(\theta, t) = M_L(\theta - \omega_0 t + \phi_L). \qquad (24)$$

The two population activities propagate with the same angular velocity, denoted by ω_0, the inhibitory population lagging after the excitatory one with a constant

phase shift. The magnitude of ω_0 as well as the shape of the profile are determined by the system parameters, as described in Appendix B. However, the sign of ω_0 – that is, the direction of the propagation of the activity profile – is arbitrary, since the underlying interactions are completely symmetric with respect to changing the spatial directions. Thus, this propagating wave exhibits a spontaneous breaking of the left/right symmetry of our system. An example of the propagating pulse is shown in Fig. 7.

How does the existence of the propagating solution depend on the model parameters? We first study the dependence on the contrast relative to thresholds, $C_L - T_L$. Throughout this work we assume that the excitatory population receives an input C_E which is above threshold. Otherwise a resting state for these neurons will be stable. Beyond this condition, the character of the solution depends on $C_L - T_L$ only through the single parameter κ, Eq. (12). For small values of κ the stable solution is the stationary one. When κ is bigger than a critical value κ_c, the stationary solution loses stability to the wave solution. The reason for this instability is the fact that increasing κ increases the component of the local inhibitory feedback relative to the excitatory one. As the inhibitory feedback becomes large, it destabilizes the stationary state and generates instead a propagating wave. This instability is also signaled by the κ-dependence of ω_c, which marks the critical frequency for locking in the marginal phase. The ratio ω_c/ϵ diverges as κ approaches κ_c from below, indicating the emergence of a spontaneously generated propagating wave. The angular velocity of the intrinsic wave, ω_0, increases with κ. For large values of κ, the stable solution becomes a homogeneous solution for which the excitatory population is quiescent and only the inhibitory neurons are active. The dependence of ω_0 on κ is shown in Fig. 8. For $\kappa < \kappa_c = -0.58$, the system reaches a stable stationary state with $\omega_0 = 0$. For $\kappa > \kappa_c$ this solution loses stability to a wave solution with $\omega_0 > 0$. As κ increases so do ω_0, θ_E and θ_I, while the mean activities m_0^E and m_0^I decrease. The plateau for high values of κ indicates a solution with a wide inhibitory activity profile, $\theta_I = 90^\circ$, where the intrinsic frequency ω_0 is independent on κ. For values of κ larger than 0.9 the stable solution is a homogeneous one, where only the inhibitory population is active. The appearance of intrinsic waves depends

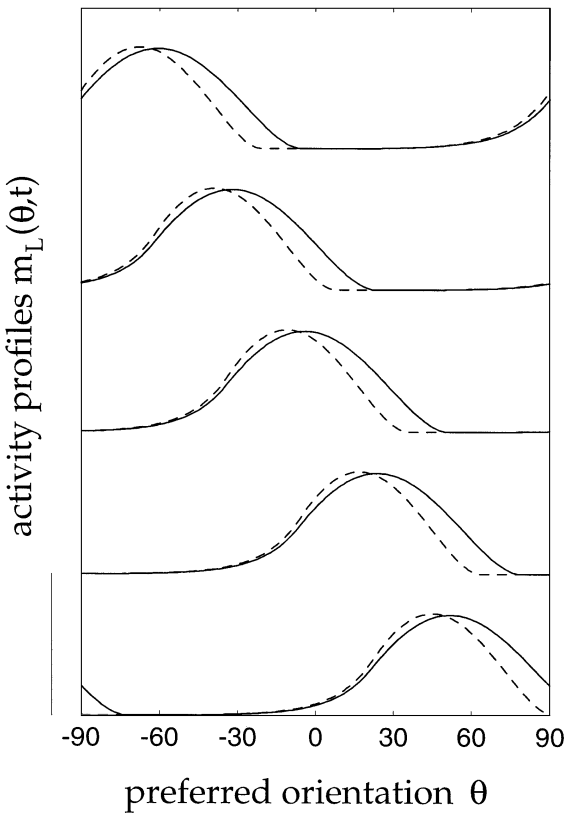

Figure 7. Intrinsic propagating waves. Solid and dashed lines are the excitatory and inhibitory activity profiles, $m_E(\theta, t)$ and $m_I(\theta, t)$, respectively, at five subsequent times separated by $2\tau_0$. The intrinsic frequency is $\omega_0 \sim 0.245$ rad/τ_0. The peak in the inhibitory activity profile, lags after the peak in the excitatory activity profile with a constant phase shift. Parameters are as in Fig. 4B, except that here $\kappa = 0$ and $\epsilon = 0$. For these parameters $\kappa_c = -0.58$. Bar is 0.1.

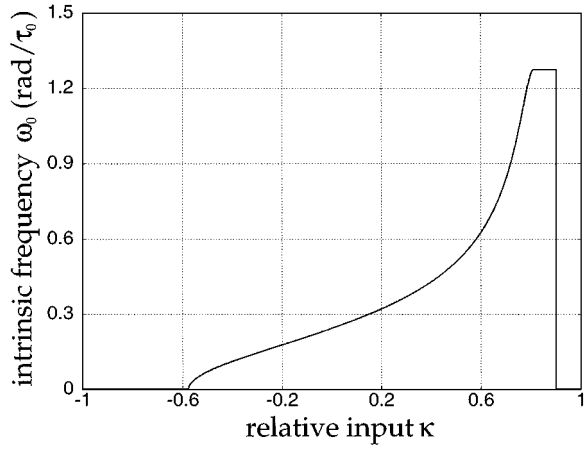

Figure 8. The intrinsic frequency ω_0 as a function of κ, the relative input to the two populations. Parameters, except for κ, are as in Fig. 4B.

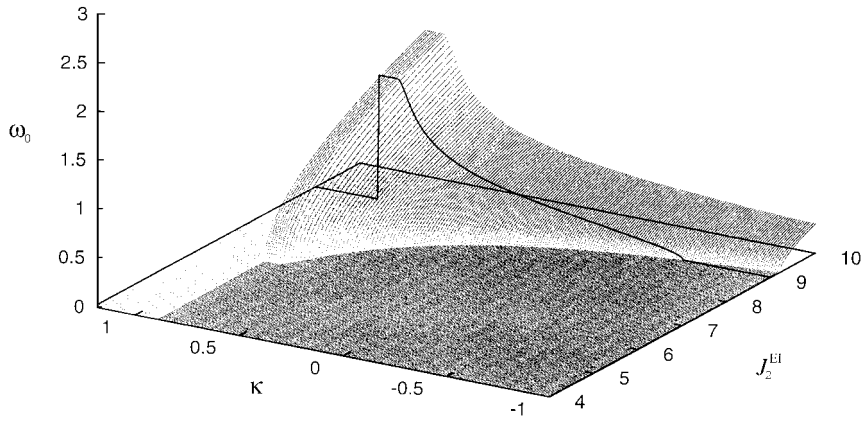

Figure 9. The intrinsic frequency ω_0 for different values of κ and J_2^{EI}. The plane $\kappa - J_2^{EI}$ is divided into three regions. Stationary region: $\kappa < 0.9$ and small J_2^{EI} (darkly shaded); Wave region: $\kappa < 0.9$ and large J_2^{EI} (not shaded); Homogeneous region: $\kappa > 0.9$ (lightly shaded). Parameters, except for κ and J_2^{EI}, are as in Fig. 4B. The solid curve is the same as in Fig. 8.

also on the parameters of the interactions $J_{LK}(\theta)$. One such parameter is J_2^{EI} (see Eq. (3)). It represents the amplitude of the spatial modulation of the inhibitory feedback onto the excitatory neurons. As mentioned above, increasing this feedback does not allow the activity in any local regime to persist. On the other hand, the excitatory input and feedback prevents the decay of the over all activity. Consequently, the instantaneous activity is locally suppressed but propagates to a nearby location. We show in Fig. 9 the phase diagram in the $\kappa - J_2^{EI}$ plane. The vertical axis denotes the magnitude of the intrinsic angular velocity, ω_0. For large J_2^{EI} there is a critical value of κ, above which the stationary solution, $\omega_0 = 0$, loses stability to a wave solution, $\omega_0 > 0$. For large values of κ the stable solution is a homogeneous one, where only the inhibitory population is active. The wave solution does not exist for small J_2^{EI}, and in this case as κ increases the stable state changes from a stationary solution directly to the homogeneous one.

5.2. *Response to Rotating Stimulus*

How does the existence of an intrinsic wave of the type described above affect the ability of the system to lock to a rotating stimulus? We expect that the system will tend to lock to a stimulus that rotates with a frequency that is near the intrinsic frequency ω_0 but will not do so when the two frequencies are far apart. This is indeed borne out by a solution of the system dynamics in the presence of a weakly tuned stimulus that rotates with frequency ω where $\omega - \omega_0 = O(\epsilon)$. Assuming once again a state of the form of Eq. (16), the dynamics of the phases can be described by

$$\frac{d\Delta_L}{dt} = -\frac{d\theta_0}{dt} + \omega_0 + \delta\omega + \omega_c \sin(2(\Delta_L - \beta_L)), \tag{25}$$

where ω_c is proportional to ϵ. Likewise, $\delta\omega$ represents an order ϵ correction to the intrinsic frequency due to the external stimulus. The phases β_L are time-independent and denote the constant phase shifts of the population profiles relative to the field $h_L(\theta, t)$ for $\epsilon = 0$ (for the derivation of this equation see Appendix C). In the case of a stimulus with constant frequency ω, the predictions of the phase equation is similar to that of the previous section. For $|\omega - \omega_0 - \delta\omega| < \omega_c$ the system is phase locked to the stimulus. The phase shifts of the populations relative to the stimulus varies from $\beta_L - \frac{\pi}{4}$ to $\beta_L + \frac{\pi}{4}$ (note that β_L is always smaller than $\frac{\pi}{4}$). Figure 10 displays the full-phase diagram that shows the regime in the ϵ-ω plane where the phase locked solution is stable. The parameters are the same as that of Fig. 6, except for κ which is above κ_c. Comparing the two phase-diagrams, we conclude that the intrinsic waves shifted the frequency regime where locking occurs to higher values.

It should be noted that the above analysis of the effect of a rotating stimulus assumes that the average frequency of the system's profile has the same sign as that of the stimulus. In general, the bistability in the direction of rotation that exists at $\epsilon = 0$ persists also for nonzero but small values of ϵ. Thus, depending on the initial conditions and the values of ϵ and ω, the

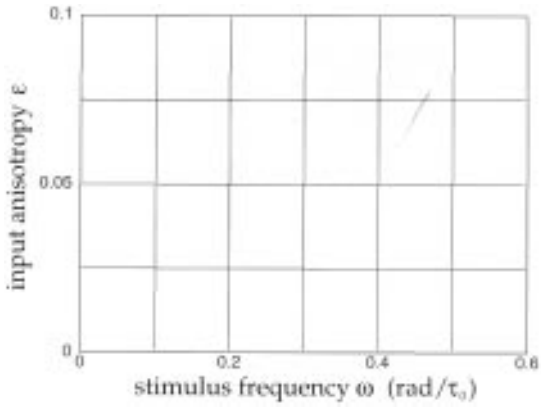

Figure 10. Phase diagram for locking to a rotating stimulus, in the intrinsic wave regime. The shaded area is the parameter regime where a phase locked solution is stable. Model parameters, except for ϵ, are as in Fig. 7. For these parameters the intrinsic stable solution that is, (for $\epsilon = 0$) is a wave with $\omega_0 \sim 0.245$ rad/τ_0.

system may settle in a state of a wave that propagates in opposite direction to the stimulus. This state is not included in Fig. 10.

6. Discussion

6.1. Summary

In this article we have explored the behavior of a network model of a cortical hypercolumn in a regime of parameters where the orientation tuning is dominated by the modulation of the cortical horizontal connections. In contrast to earlier studies (Ben-Yishai et al., 1995a; Somers et al., 1995; Hansel and Sompolinsky, 1996a) we have focused here on the spatiotemporal domain. Specifically, we have examined scenarios where the stable state of the system is a moving hill of activity, rather than a stationary hill. We first studied the conditions under which the population activity profile will follow a visual stimulus that rotates around its center within a single receptive field. Our analysis predicts that for low-stimulus rotation frequencies the system will respond with a sharply tuned profile of activity, which will follow the stimulus with a constant phase lag. For stimulus frequencies above a critical frequency ω_c, the population activity profile will lag in frequency and will execute a quasi-periodic motion. The second scenario for a moving profile in our model is the spontaneous appearance of propagating waves due to the destabilization of the stationary state.

6.2. The Basic Assumptions of the Work

Our results are based on the central assumptions that (1) the anisotropy of the input from the LGN to the cortex induced by the stimulus is weakly tuned (that ϵ of Eq. (8) is small), and (2) even in such conditions, the cortical responses are sharply tuned, due to the local cortical interactions. In our model ϵ is a global parameter. In reality, there is apparently a substantial variation in the degree of tuning of the afferent input to different cortical sites (Chapman et al., 1991), which makes it hard to compare directly to the model. As stated in the Introduction, one way of satisfying the condition of weakly tuned input is by controlling the anisotropy of the visual stimulus itself. Thus, an important test of the hypothesis of cortical participation in orientation tuning would be to measure the width of the tuning as a function of the stimulus anisotropy, such as by varying the aspect ratio of the visual stimulus. According to our hypothesis, a weakly anisotropic stimulus will generate a sharply tuned response with an amplitude that varies smoothly with its contrast. It should be noted, however, that in reality for very small anisotropy the spontaneously generated profile of activity will wander across the hypercolumn because of the noise in the neuronal activity, which has been neglected in our mean-field equations. Such a wandering will occur also in the absence of noise if the spontaneously generated pattern is a traveling wave. In this case, a minimal positive value of ϵ is needed in order to "pin" the activity profile to the stimulus orientation as is seen in Fig. 10. Hence, for very small ϵ the *average* level of activity will be substantially reduced.

We have also assumed in our present analysis that the input has a relatively broad shape, even for large ϵ (see Eq. (8)). This assumption is made primarily for convenience of analysis. A more general form for $h_L^{\text{ext}}(\theta)$ including a narrower profile will not change qualitatively our present results as long as the overall spatial modulation of the input is small. This modulation can be parametrized by say, the total power of its nonzero Fourier-components relative to the zero-th component. The above is valid as long as $h_L^{\text{ext}}(\theta)$ has the general shape assumed here – namely, it is symmetric around a unique maximum.

Throughout this work we have assumed that the activation of the excitatory population by the stimulus is suprathreshold – that $C_E > T_E$. If the excitatory population has subthreshold activation, then the state where all the excitatory population is quiescent is a stable

state, which is of course not interesting. On the other hand, the inhibitory population may be active (due to the excitatory input from the network) even if the stimulus is subthreshold. Hence, the parameter κ, Eq. (12) was allowed to assume negative as well as positive values; see the phase diagram of Fig. 9. The precise range of κ where the different transitions occur depends on the other model parameters; hence our model does not tightly constrain its value. At present, it is hard to estimate the value of κ from experiment, since relatively little is known about the distribution of thresholds and contrast gain of inhibitory neurons in primary visual cortex. Models that rely on feedforward inhibition in cortex, for example, direction selectivity, may favor the assumption of suprathreshold activation of inhibitory neurons, perhaps even stronger than that of excitatory neurons. On the other hand, recent models of "surround effects" on RFs argue in favor of inhibitory neurons having a considerable less activation by stimulus than the excitatory ones (Stemmler et al., 1995; Somers et al., 1996).

In our previous work (Ben-Yishai et al., 1995a), we have focused on a network with stable stationary states; hence it was sufficient to consider a parameter regime where the inhibitory and excitatory populations are identical, in which case the network can be described in terms of a single activity profile. In this reduced network intrinsic waves cannot exist due to the symmetry of the connection matrix. Here we have considered a more general architecture in which the two populations are distinct. In this case the connection matrix is not symmetric and time-dependent attractors can exist.

Previously, we have pointed out that the cortical mechanism for orientation tuning explains the experimentally observed separability of the coding of the stimulus orientation and contrast. In the model we have investigated, changing the stimulus contrast (above threshold) changes the overall amplitude of the tuning curve but does not change its width, which was determined by the spatial modulation of the cortical interactions. The present work shows that the separability of contrast and orientation dimensions is carried over to the spatiotemporal domain. However, due to the presence of two nonequivalent populations, the effect of changing the contrast is more subtle. If the two populations receive the same activation $C_L = C$ and have the same thresholds $T_L = T$, then although their connectivity profiles may be different, changing C will result in an overall scaling of the activity profiles without changing either the shapes of the profile nor their motion. In the case of different C_L or T_L, then strictly speaking, invariance of shape or motion is achieved only if both C_L and T_L are scaled by the same factor. Thus, in general a change in the stimulus contrast alone will modify the *relative* levels of input to the two populations, κ, and hence in principle may change the statics or the dynamics of the profile. In fact, we have found that κ affects, albeit weakly, the width of the tuning curve.

Our dynamic model is similar to dynamic equations used previously to model the behavior of large neuronal populations (Wilson and Cowan, 1972; Freeman, 1975). It ignores the highly nonlinear dynamics of spikes, the temporal fluctuations in the activity are averaged out, and synaptic inputs are modeled as currents. These simplifications are justified because we focus here on dynamical processes that are slow compared to the single-cell time constant and are dominated by smooth cooperative effects. In the case studied in Section 4 the restriction to slow dynamics was explicitly assumed, since our phase model was limited to $\omega\tau_0 \propto \epsilon \ll 1$. However, the above considerations imply that our theory of the intrinsic wave, Section 5, is justified only when the intrinsic frequency ω_0 is small – that is, that the system is near the bifurcation point $\kappa = \kappa_c$ (see Fig. 8).

6.3. Locking to Rotating Stimulus

The existence of distinct regimes of frequency and phase locking in our system is similar to that observed in low-dimensional oscillatory systems that are forced by an oscillatory external force (Glass and Mackey, 1988; Knight, 1972). In general, the temporal relation between the oscillator and the force may be complex. Here we have focused on parameter regimes where the stable spatiotemporal patterns are relatively simple. They consist of an activity profile that is time-independent in a reference frame that moves with it. In general, the shape of the profile depends on the stimulus parameters such as ω and ϵ. However, when ϵ and the difference between ω and the intrinsic frequency are both small, the shape of the profile is essentially the same as that without an oriented stimulus. This leads to a relatively simple-phase dynamic equations that describe the evolution in time of the locii of the activity profiles, Eqs. (18) and (25). Phase models have been applied successfully also in several neuronal

models. Examples are models of the high-frequency γ oscillations in cat visual cortex (Schuster and Wagner, 1990a, 1990b; Sompolinsky et al., 1991; Grannan et al., 1993) and the propagating waves in lamprey (Williams et al., 1990). Phase models have been also used to investigate theoretically the conditions (cell and synaptic properties) under which oscillating neurons can synchronize their activities in small and large neuronal systems (Hansel et al., 1995; Van Vreeswijk et al., 1995). These studies considered the locking of oscillating neurons or neuronal populations, by weak coupling. In contrast, in the case studied in Section 4, the network did not oscillate at all in the absence of the stimulus but approached a stationary profile. Locking to the rotating stimulus was, nevertheless, possible due to the marginality (for $\epsilon = 0$) of the stationary phase – namely, the existence of a continuum of attractors with identical spatial profiles.

6.4. *Mechanism for the Appearance of Intrinsic Waves*

A main finding of our work is that intrinsic rotation of the activity profile can occur in a simple model of a hypercolumn even if the lateral connections are symmetric with respect to spatial direction. Thus, whereas the magnitude of the rotation frequency is determined uniquely by the network parameters, the sign of the rotation (that is, clockwise or counterclockwise) is arbitrary and is selected by the initial conditions of the network. In contrast, other network models (Lukashin et al., 1995) for generating moving-activity profiles in similar hypercolumn architectures rely on spatial asymmetry in the connections, which "push" the activity in the direction of increasing excitatory connections (or decreasing inhibitory ones). An interesting consequence of the bistability of the network in this parameter regime is that even in the presence of an external rotating input, the network may exhibit a propagating wave in a direction that is opposite to the direction of rotation of the stimulus.

Our results regarding the intrinsic waves suggest that application of nonoriented stimulation will induce cortical activity that may include moving "spots" across different orientation columns. Previous numerical simulations of large neural networks with excitatory and inhibitory feedback connections have revealed complex spatiotemporal patterns of activation including "hotspots" that execute a "random walk motion" across the network (see e.g., Usher et al., 1994). Our results imply that the motion of these spots will have a significant component that will periodically activate different orientation columns.

In the present model, the waves appear due to the existence of strong local inhibitory feedback. A "spot" of activity at one location is inhibited by this negative feedback, but the level of excitation is sufficiently strong to prevent the decay of the overall activity. The system is forced to move the spot of activity to a nearby location (either to the right or to the left of the present one). This mechanism requires a spatially modulated inhibition, and will not work in – for example, a network with *global* inhibition. In a recent work (Hansel and Sompolinsky, 1996b), we have found that neuronal adaptation, not included in the present model, provides another mechanism for the generation of intrinsic waves in a cortical module with an architecture similar to the present one. In this case, waves appear even if the inhibition is global and serves only to control the overall level of activity.

From a dynamic point of view the mechanism for generating waves in our model is similar to the well-known phenomenon of spontaneous appearance of propagating pulses in one-dimensional reaction-diffusion systems (Rinzel and Keller, 1973; Murray, 1989; Cross and Hohenberg, 1993). Our system is simpler in that the interactions, although spatially modulated, are long-ranged; hence the waves can be described by nonlinear equations of few order parameters rather than by nonlinear differential equations, which are necessary in physical systems governed by short-range interactions. The onset of traveling fronts and pulses in one-dimensional neural networks has been also investigated by Idiart and Abbott (1993). In their model the mechanism for traveling waves involved explicit delays in the interactions. In addition, their model has open boundary conditions and therefore the spatiotemporal patterns are transient. In contrast, in our model the effective delayed feedback is generated by the inhibitory neurons and the spatiotemporal patterns are attractors of the dynamics.

6.5. *Functional Implications*

We now discuss some possible functional implications of the network dynamic behavior. A simple ansatz is that the system encodes information about a stimulus orientation $\theta_0(t)$ simply in the value of the phase of the excitatory population vector $\psi_E(t - \tau_d)$, where the τ_d represents an appropriate constant delay time. Then,

our results concerning locking to a rotating stimulus in the marginal phase imply that for low frequencies the system is able to faithfully transmit the information about a time-dependent external angle, even when the signal to noise ratio of the stimulus orientation is small. In this context, a possible advantage of the existence of intrinsic waves in an appropriate parameter regime is that they shift the range of frequencies for which locking to a rotating stimulus occurs to higher values – namely, to a band of frequencies near the intrinsic frequency of the system. For frequencies outside the regime where full locking occurs the amount of lost information about the stimulus is represented by the width of the distribution of the difference between the instantaneous angles of the population vector and the stimulus, see Fig. 5. Additional possibilities exist if the information about the stimulus is extracted in more complex manners. For instance, fast intrinsic waves can encode the position of a slowly moving stimulus using an appropriate periodic resetting signal, as was suggested recently for the temporal coding of place in the hippocampus (Tsodyks et al., 1995).

6.6. *Experimental Aspects*

Electrophysiological measurements in visual cortex can test the theoretical predictions about the response of the system to a rotating visual stimulus. It should be noted however that in reality there is an inherent delay between the visual stimulus and the resultant input to the cortex from the LGN, which is not incorporated in our model. Thus, only predictions about the *relative phases* between the stimulus and the population vector are meaningful. The response of neurons to rotating visual patterns have been measured in extrastriatal visual areas, in particular in area MST (Tanaka and Saito, 1989; Tanaka et al., 1989). These experiments focus primarily on the selectivity to the direction of rotation. Indeed, it was found that some neurons respond selectively to clockwise or counterclockwise rotations. We are not aware of measurements of responses of neurons in V1 to rotating stimuli within their receptive fields. A natural way of observing the motion of the activity profile in a hypercolumn is by means of the *population vector*. In fact, it is well known that constructing the population vector yields a plausible mechanism for *reading out* the angle information from a population of noisy, broadly tuned neurons. Under certain conditions, the population vector is asymptotically the optimal angle estimator (Seung and Sompolinsky, 1993; Salinas and Abbott, 1994). It is interesting that the population vector is in fact the natural time-dependent order parameter in our theory. The population vector of the neuronal responses in V1 can be measured experimentally by sampling single unit responses time-locked to a rotating stimulus. Alternatively, optical imaging techniques (Grinvald et al., 1984; Orbach et al., 1985) may be used to construct the population vector from the large-scale spatiotemporal pattern of electrical activity evoked by a rotating stimulus.

Visual perception is another potential testing ground of our predictions. Previously, we have considered the response of the system to an abrupt switching of the stimulus orientation (Ben-Yishai et al., 1995a). We have shown that in the marginal phase the population profile travels slowly from its original position to the new location, in a manner that mimics the response to a slowly rotating stimulus. This *virtual rotation* may be related to the perceptual phenomenon of *apparent rotational motion* when subjects are presented with alternating visual patterns (Finke and Shepard, 1984). The present work deals with the case of a stimulus that changes smoothly its orientation. Thus, it might be possible to test our predictions regarding the dependence of the locking to external stimulus on the stimulus frequency ω and anisotropy ϵ, by psychophysical measurements of the perception of rotating stimuli and its dependence on such parameters.

6.7. *Concluding Remarks*

In this work we have focused on a network model of the local cortical circuits in the primary visual cortex. However, many of the issues and the results of our work are relevant to the behavior of local neuronal networks in other systems as well. A closely related system is the assembly of neurons that are selective to the direction of voluntary arm movements in the motor cortex. The application of our approach to the coding of movement trajectories in the motor cortex is currently being studied (Ben-Yishai et al., 1995b). The representation of eye-movement in the superior-colliculus is another area where our approach can be used. Recent studies of the waves of electrical activity in the procerebral lobe of the terrestrial mollusc *Limax* indicate that odor signals modulate primarily the spatial distribution of phases of the underlying activity oscillations, and to a lesser extent their frequency (Kleinfeld et al., 1994). This may be analogous to the effect of an external stimulus on the intrinsic propagating waves in our network.

Appendix A

For a stimulus with a time-dependent orientation, the general equations are

$$h_L^{\text{ext}}(\theta, t) = C_L\,[1 - \epsilon\ +\ \epsilon\cos\,(2(\theta - \theta_0(t)))] \qquad 0 \le \epsilon \le 0.5. \quad (26)$$

The total inputs to the two populations are

$$h_L(\theta, t) = h_L^0(t) + H_L(t)\cos(2(\theta - \alpha_L(t))) \quad (27)$$

$$h_L^0(t) = J_0^{LE} m_0^E - J_0^{LI} m_0^I + C_L(1-\epsilon) - T_L \quad (28)$$

and $H_L(t)$ and $\alpha_L(t)$ are defined by

$$H_L(t)e^{2i\alpha_L(t)} = \epsilon C_L e^{2i\theta_0(t)} + J_2^{LE} m_2^E e^{2i\psi_E} - J_2^{LI} m_2^I e^{2i\psi_I}. \quad (29)$$

$h_L(\theta, t)$ can be written as

$$h_L(\theta, t) = H_L(t)\,[\cos(2(\theta - \alpha_L(t))) - \cos(2\theta_L(t))], \quad (30)$$

where the tuning width angles θ_L are defined by the condition

$$h_L(\alpha_L(t) \pm \theta_L(t)) = 0 \quad (31)$$

yielding

$$\cos(2\theta_L(t)) = \frac{-h_L^0(t)}{H_L(t)}. \quad (32)$$

Note that $2\theta_L$ is the width of the region where the total input to the neurons is above threshold. The order parameters m_0^L, m_2^L, and ψ_L are defined in Eqs. (5) and (6). Integrating Eq. (1) over θ, with and without a factor $e^{2i\theta}$, yields

$$\tau_0 \frac{d}{dt} m_0^L = -m_0^L + H_L\, f_0^L(\theta_L(t)) \quad (33)$$

$$\tau_0 \frac{d}{dt} m_2^L = -m_2^L + H_L(t)\, f_2(\theta_L(t))\cos(2(\alpha_L(t) - \psi_L(t))) \quad (34)$$

and

$$2m_2^L \tau_0 \frac{d}{dt}\psi_L = H_L\, f_2(\theta_L(t))\sin(2(\alpha_L(t) - \psi_L(t))) \quad (35)$$

where

$$f_0(x) = \frac{1}{\pi}\Big(\sin(2x) - 2x\cos(2x)\Big) \quad (36)$$

$$f_2(x) = \frac{1}{\pi}\Big(x - \frac{1}{4}\sin(4x)\Big). \quad (37)$$

In the following we write $f_n^L = f_n(\theta_L)$.

We now give the details of the mean-field equations that determine the profiles of activity of the two populations in the stationary inhomogeneous state for a stationary stimulation—that is, θ_0 is time independent and the stationary profile is given by Eq. (7). In this case,

$$h_L(\theta) = h_L^0 + H_L\cos(2(\theta - \alpha_L)) \quad (38)$$

$$h_L^0 = J_0^{LE} m_0^E - J_0^{LI} m_0^I + C_L(1-\epsilon) - T_L \quad (39)$$

$$\alpha_L = \psi_L = \theta_0, \quad (40)$$

which here we take as $\theta_0 = 0^\circ$, and

$$H_L = \epsilon C_L + J_2^{LE} m_2^E - J_2^{LI} m_2^I. \quad (41)$$

To evaluate the order parameters m_0^L and m_2^L we note that the population profiles are given by

$$m_L(\theta) = \begin{cases} H_L\,(\cos\,(2\theta) - \cos\,(2\theta_L)) & |\theta| < \theta_L \\ 0 & |\theta| > \theta_L \end{cases} \quad (42)$$

The order parameters are

$$m_0^L = H_L\, f_0^L \qquad L = E, I \quad (43)$$

$$m_2^L = H_L\, f_2^L \qquad L = E, I \quad (44)$$

Substituting Eqs. (43) and (44) into Eq. (41) yields linear equations for H_L for given θ_L. To complete the solution we have to determine the values of θ_L. To do this we use Eq. (32) and obtain a nonlinear equation for θ_L.

In the limit $\epsilon = 0$, Eq. (41) are homogeneous linear equations in H_L. The condition that they have a

non-trivial solution – that is, one with $H_L \neq 0$, is

$$\left(J_2^{II} f_2^I + 1\right)\left(J_2^{EE} f_2^E - 1\right) - J_2^{IE} J_2^{EI} f_2^E f_2^I = 0. \tag{45}$$

This equation determines a relation between the two angles θ_L. Depending on the values of the interaction parameters, J_2^{KL}, it may not have a solution. In that case the only stationary solution is $H_L = 0$ – that is, $m_L(\theta)$ is constant. On the other hand, there is a considerable range of parameters for which a solution to Eq. (45) exists. In such a case, Eq. (41) determine only the ratio between H_E and H_I. However, now, the two equations Eq. (32) together with Eq. (45) determine both the angles and the overall magnitude of H_L. This completes the solution of the marginal phase. In this state, the angle $\psi = \psi_E = \psi_I$ is arbitrary, reflecting the rotational invariance of the system.

Appendix B

In this Appendix, we sketch the derivation of the equations that determine the conditions of locking to a rotating stimulus and the properties of the locked state.

We assume a stimulus of the form

$$h_L^{\text{ext}}(\theta, t) = C_L(1 - \epsilon + \epsilon \cos(2(\theta - \omega t))) \tag{46}$$

and look for a solution of the form

$$m_L(\theta, t) = M_L(\theta - \omega t - \Delta_L), \tag{47}$$

where $\Delta_L = \psi_L(t) - \omega t$ is time-independent. This angle measures the angular shift between the motion of the population profile and the orientation of the rotating stimulus. Substituting this equation in (1) leads to a pair of differential equations for $M_L(\theta)$:

$$-\omega\tau_0 \frac{d}{d\theta} M_L(\theta) = -M_L(\theta) + g(h_L(\theta)), \tag{48}$$

where $h_L(\theta)$ is given by

$$h_L(\theta) = h_L^0 + H_L \cos(2(\theta - \gamma_L - \omega t)) \tag{49}$$

$$H_L e^{2i\gamma_L} = \epsilon C_L + J_2^{LE} m_2^E e^{2i\Delta_E} - J_2^{LI} m_2^I e^{2i\Delta_I} \tag{50}$$

(see Eq. (29)). Note that here γ_L is the time-independent angle that corresponds to the peak of the total input relative to ωt, related to $\alpha_L(t)$ by $\gamma_L = \alpha_L(t) - \omega t$. Fourier transforming Eq. (48) one derives the following equations ($L = E, I$) for the order parameters

$$m_0^L = H_L f_0^L \tag{51}$$

$$m_2^L = \frac{H_L}{\sqrt{1 + 4\omega^2}} f_2^L \tag{52}$$

$$\tan 2(\gamma_L - \Delta_L) = 2\omega, \tag{53}$$

where f_0^L and f_2^L are defined in Eqs. (36) and (37), respectively. Substituting (51) and (52) in Eq. (50), leads to a system of four equations determining H_L and γ_L, in terms of Δ_L and θ_L. The angles Δ_L are determined by Eq. (53) and θ_L by Eq. (32), which completes the evaluation of the order parameters. For a given ϵ a solution to this system of equations exists in a range of values of ω that defines the range of the rotation frequency of the stimulus to which the activity of the network can lock. Finally, the complete activity profiles are evaluated by solving Eq. (48), yielding

$$M_L(\theta) = \begin{cases} a_L e^{\theta/\omega} & \theta - \gamma_L < -\theta_L \\ b_L e^{\theta/\omega} + \frac{H_L}{\sqrt{1+4\omega^2}} \cos(2\theta) & \\ \qquad - H_L \cos(2\theta_L) & |\theta - \gamma_L| \leq \theta_L \\ a_L e^{(\theta-\pi)/\omega} & \theta - \gamma_L > \theta_L. \end{cases} \tag{54}$$

The condition that M_L is continuous at $\theta = \gamma_L \pm \theta_L$ determines the coefficients a_L and b_L. Note that M_L is always strictly positive. This is unlike the case of $\omega = 0$ for which the activity of the neurons is 0 for $|\theta| > \theta_L$.

In the limit $\epsilon = 0$ the four linear equations derived from (50) are homogeneous. The condition that this system has a nontrivial solution for H_L corresponds to three determinantal equations that relate the synaptic strengths to the angles γ_L and Δ_L. Equations (50) yield a fourth equation for the ratio $\frac{H_I}{H_E}$. Since for $\epsilon = 0$ the origin of the angles can be chosen arbitrarily we will fix $\Delta_E = 0$. Therefore one has a system of eight coupled equations, to determine the seven unknowns θ_L, γ_L, Δ_I, and H_L. In general there is no solution to this set of equations except for a particular value of ω. This value is the frequency ω_0 of the spontaneous traveling pulse.

Appendix C

In this Appendix we derive the phase equation Eq. (18). We assume that ϵ is small and that the parameters and the contrasts C_L are such that the network would be in a stationary marginal state if $\epsilon = 0$. We also assume that the angular velocity of the stimulus is small – that is,

$$\frac{d\theta_0}{dt} = O(\epsilon). \tag{55}$$

In this case, the derivative with respect to time of all order parameters are of order ϵ. In addition, the following ansatz is made (to leading order in ϵ):

$$\psi_E(t) - \psi_I(t) = \epsilon\, \bar{\psi}(t) \tag{56}$$

$$\alpha_L(t) - \psi_L(t) = \epsilon\, \bar{\alpha}(t) \tag{57}$$

$$\psi_L(t) - \theta_0(t) = \Delta(t). \tag{58}$$

$\bar{\psi}(t)$, $\bar{\alpha}(t)$, and $\Delta(t)$ are functions of time, of order 1, with time derivatives which are of order ϵ. Substituting this Ansatz in Eq. (29) we obtain the following equations:

$$H_E(t)e^{2i\epsilon\bar{\alpha}} = \epsilon C_E e^{-2i\Delta} + J_2^{EE} m_2^E - J_2^{EI} m_2^I e^{-2i\epsilon\bar{\psi}} \tag{59}$$

$$H_I(t)e^{2i\epsilon\bar{\alpha}} = \epsilon C_I e^{-2i\Delta} + J_2^{IE} m_2^E e^{2i\epsilon\bar{\psi}} - J_2^{II} m_2^I. \tag{60}$$

Taking the imaginary part of these equations and expanding the resulting equations to order ϵ we obtain,

$$\epsilon\bar{\alpha}(t) = \omega_c \sin(2\Delta(t)), \tag{61}$$

where,

$$\omega_c = \epsilon \frac{\left(1 + J_2^{II} f_2^I\right) C_E - J_2^{EI} f_2^I C_I}{2H_E\left(J_2^{EE} f_2^E - J_2^{II} f_2^I - 2\right)}. \tag{62}$$

Finally, from Eq. (35) we obtain to leading order

$$\frac{d\psi_L}{dt} = \epsilon\bar{\alpha}(t), \tag{63}$$

where we have used Eq. (34) with $\frac{dm_2^L}{dt} = 0$. Hence, using the definition of $\Delta(t)$ we obtain

$$\frac{d\Delta}{dt} = -\frac{d\theta_0}{dt} + \omega_c \sin(2\Delta). \tag{64}$$

A similar method can be applied in the intrinsic wave regime to derive Eq. (25).

Acknowledgments

We thank D. Golomb, P.C. Hohenberg, D. Kleinfeld, and D.W. Tank for helpful discussions. D.H. acknowledges the very warm hospitality of the Racah Institute of Physics and the Center for Neural Computation of the Hebrew University. We thank the anonymous referees for very helpful comments. We acknowledge the hospitality of the Marine Biological Laboratory, Woods Hole, during the summer of 1995, where part of the work was concluded. D.H. was supported in part by the PICS-CNRS (PIR Cognisciences and M.A.E): "Dynamique neuronale et codage de l'information: Aspects physiques et biologiques".

References

Ahmed B, Douglas RJ, Martin KAC, Nelson JC (1994) Map of the synapses formed with the dendrites of spiny stellate neurons in cat visual cortex. *J. Comp. Neurol.* 341:16–24.

Barlow HB, Levick WR (1965) The mechanism of directionally selective units in rabbit's retina. *J. Physiol.* 178:477–504.

Ben-Yishai R, Hansel D, Sompolinsky H (1995b) Traveling waves and coding of movement in a cortical network module. Proceedings of the Annual Meeting of the Israel Society for Neurosciences. *Israel J. Med. Sci.* 31:772.

Ben-Yishai R, Lev Bar-Or R, Sompolinsky H (1995a) Theory of orientation tuning in visual cortex. *Proc. Natl. Acad. Sci. (USA)* 92:3844–3848.

Celebrini S, Thorpe S, Trotter Y, Imbert M (1993) Dynamics of orientation coding in area V1 of the awake primate. *Visual Neurosci.* 10:811–825.

Chapman B, Zahs KR, Stryker MP (1991) Relation of cortical cell orientation selectivity to alignment of receptive fields of the geniculocortical afferents that arborize within a single orientation column in Ferret visual cortex. *J. Neurosci.* 11:1347–1358.

Cross MC, Hohenberg P (1993) Pattern formation outside of equilibrium. *Rev. Mod. Phys.* 65:851–1112.

Chagnac-Amitai Y, Connors BW (1989) Horizontal spread of synchronized activity in neocortex and its control by GABA-mediated inhibition. *J. Neurophysiol.* 61:747–758.

Dinse HR, Kruger K, Best J (1990) A temporal structure of cortical information processing. *Concepts in Neurosci.* 1:199–238.

Douglas RJ, Koch C, Mahowald M, Martin K, Suarez H (1995) Recurrent excitation in neocortical circuits. *Science* 269:981–985.

Ermentrout GB, Mc Leod JB (1993) Existence and uniqueness of traveling waves for a neuronal network. *Proc. Royal Society of Edinburgh* 123A:461–478.

Ferster D (1986) Orientation selectivity of synaptic potentials in neurons of cat primary visual cortex. *J. Neurosci.* 6:1284–1301.

Ferster D, Chung S, Wheat H (1996) Orientation selectivity of thalamic input to simple cells of cat visual cortex. *Science* 380:249–252.

Ferster D, Koch C (1987) Neuronal connections underlying orientation selectivity in cat visual cortex. *Trends in Neurosci.* 10:487–492.

Finke RA, Shepard RN (1984) Visual functions of mental imagery. In: KR Boff, L Kaufman, JP Thomas, eds. Handbook of Perception and Human Performance, Wiley, New York, vol. 2.

Freeman W (1975) Mass Action in the Brain. Academic, New York.

Georgopoulos AP (1995) Current issues in directional motor control. *Trends in Neurosci.* 18:506–510.

Georgopoulos AP, Kettner RE, Schwartz AB (1988) Primate motor cortex and free arm movements to visual targets in three-dimensional space. II. Coding of the direction of movement by a neuronal population. *J. Neurosci.* 8:2928–2937.

Georgopoulos AP, Taira M, Lukashin A (1993) Cognitive neurophysiology of the motor cortex. *Science* 260:47–52.

Glass L, Mackey MC (1988) From Clocks to Chaos: The Rhythms of Life. Princeton University Press, Princeton, NJ.

Golomb D, Wang XJ, Rinzel J (1996) Propagation of spindle waves in a thalamic slice model. *J. Neurophysiol.* 75:750–769.

Grannan ER, Kleinfeld D, Sompolinsky H (1993) Stimulus-dependent synchronization of neuronal assemblies. *Neural Comp.* 5:550–569.

Grinvald A, Anglister L, Freeman JA, Hildesheim R, Manker A (1984) Real-time optical imaging of naturally evoked electrical activity in the intact frog brain. *Nature* 308:848–850.

Guitton D (1992) Control of eye-head coordination during orienting gaze shifts. *Trends in Neurosci.* 15(5):174–179.

Gutnick MJ, Connors BW, Prince DA (1982) Mechanisms of neocortical epileptogenesis in vitro. *J. Neurophysiol* 48:1321–1335.

Hansel D, Mato G, Meunier C (1995) Synchronization in excitatory neural networks. *Neural Comp.* 7:307–338.

Hansel D, Sompolinsky H (1996a) Chaos and synchrony in a model of a hypercolumn in visual cortex. *J. Comput. Neurosci.* 3:7–34.

Hansel D, Sompolinsky H (1996b) The role of adaptation in spatiotemporal dynamics of cortical neural networks. In preparation.

Hata Y, Tsumoto T, Sato H, Hagihara K, Tamura H (1988) Inhibition contributes to orientation selectivity in visual cortex of cat. *Nature* 335:815–817.

Hubel DH, Wiesel TN (1962) Receptive fields, binocular interaction and functional architecture in the cat's visual cortex. *J. Physiol. Lond.* 160:106–154.

Idiart MAP, Abbott LF (1993) Propagation of excitation in neural network models. *Network* 4:285–294.

Kim U, Bal T, McCormick DA (1995) Spindle waves are propagating synchronized oscillations in the ferret LGNd in vitro. *J. Neurophysiol.* 74:1301–1323.

Kleinfeld D, Delaney KR, Fee MS, Flores JA, Tank TW, Gelperin A (1994) Dynamics of propagating waves in the olfactory network of a terrestrial mollusc: An electrical and optical study. *J. Neurophysiol.* 72:1402.

Knight BW (1972) Dynamics of encoding in a population of neurons *J. Gen. Physiol.* 56:734–767.

Kuramoto Y (1984) Chemical Oscillations, Waves and Turbulence. Springer-Verlag, New York.

Laurent G, Naraghi M (1994) Odorant-induced oscillations in the mushroom bodies of the locust. *J. Neurosci.* 14:2993–3004.

Li Z, Hopfield JJ (1989) Modeling the olfactory bulb and its neural oscillatory processings. *Biol. Cybern.* 61:379–392.

Lukashin AV, Georgopoulos AP (1993) A dynamical neural network model of motor cortical activity during movement: Population coding of movement trajectories. *Biol. Cyber.* 69:517–524.

Lukashin AV, Wilcox GL, Georgopoulos AP (1995) Modeling of directional operations in the motor cortex: a noisy network of spiking neurons is trained to generate neural-vector trajectories. Preprint.

Maex R, Orban GA (1992) A model circuit for cortical temporal low-pass filtering. *Neural Comput.* 4:932–945.

Martin KAC (1988) From single cells to simple circuits in the cerebral cortex. *Q. J. Exp. Physiol.* 73:637–702.

Miles R, Traub RD, Wong RKS (1988) Spread of synchronization firing in longitudinal slices from the CA3 region of the hippocampus. *J. Neurophysiol.* 60:1481–1496.

Munoz D, Pelisson D, Guitton D (1991) Movement of neural activity on the superior colliculus motor map during gaze shifts. *Science* 251:1358–1360.

Murray JD (1989) Mathematical Biology. Springer, Berlin.

Nelson S, Toth L, Sheth B, Sur M (1994) Orientation selectivity of cortical neurons during intra-cellular blockade of inhibition. *Science* 265:774–777.

Orbach HS, Cohen LB, Grinvald A (1985) Optical mapping of electrical activity in rat somatosensory and visual cortex. *J. Neurosci.* 5:1886–1895.

Orban GA (1984) Neuronal operations in the visual cortex. Springer, Berlin.

Pei X, Vidyasagar TR, Volgushev M, Creutzfeldt OD (1994) Receptive field analysis and orientation selectivity of postsynaptic potentials of simple cells in cat visual cortex. *J. Neurosci.* 14:7130–7140.

Reid RC, Alonso JM (1995) Specificity of monosynaptic connections from thalamus to visual cortex. *Nature* 378:281–284.

Rinzel J, Keller JB (1973) Traveling wave solutions of a nerve conduction equation. *Biophys. J.* 13:1313–1337.

Salinas E, Abbott LF (1994) Vector reconstruction from firing rates. *J. Comput. Neurosci.* 1:89–107.

Schuster HG, Wagner P (1990a) A model for neuronal oscillations in the visual cortex. I. Mean field theory and the derivation of the phase equations. *Biol. Cybern* 64:77–82.

Schuster HG, Wagner P (1990b) A model for neuronal oscillations in the visual cortex. II. Phase description of the feature dependent synchronization. *Biol. Cybern* 64:83–85.

Schwartz AB (1993) Motor cortical activity during drawing movements: Population representation during sinusoid tracing. *J. Neurophysiol.* 70:28–36.

Seung HS, Sompolinsky H (1993) Simple models for reading neuronal population codes. *Proc. Natl. Acad. Sci.* 90:10749–10753.

Shevelev A, Novikova RV, Lazareva NA, Tikhomirov AS, Sharaev GA (1995) Sensitivity to cross-like figures in the cat striate neurons. *Neurosci.* 69:51–57.

Sillito AM (1977) Inhibitory process underlying the directional specificity of simple, complex and hypercomplex cells in cat's visual cortex. *J. Physiol.* 271:699–720.

Sillito AM, Kemp JA, Milson JA, Berardi N (1980) A re-evaluation of the mechanisms underlying simple cell orientation selectivity. *Brain Res.* 194:517–520.

Somers D, Nelson S, Sur M (1995) An emergent model of orientation selectivity in cat visual cortical simple cells. *J. Neurosci.* 15:5448–5465.

Somers D, Toth LJ, Todorov E, Chenchal-Rao S, Kim D, Nelson SB, Siapas AG, Sur M (1996) Variable gain control in local cortical circuitry supports context-dependent modulation of long-range connections. In: J Sirosh, R Miikkulainen, eds. Lateral Interactions in the Cortex. University of Texas, Austin.

Sompolinsky H, Golomb D, Kleinfeld D (1991) Cooperative dynamics of visual processing. *Phys. Rev.* A43:6990–7011.

Stemmler M, Usher M, Niebur E (1995) Lateral interactions in primary visual cortex: A model bridging physiology and psychophysics. *Science* 269:1877–1880.

Suarez H, Koch C, Douglas R (1995) Modeling direction selectivity of simple cells in striate visual cortex within the framework of the canonical microcircuit. *J. Neurosci.* 15:6700–6719.

Tanaka K, Fukuda Y, Saito H (1989) Underlying mechanisms of the response specificity of expansion/contraction, and rotation cells in the dorsal part of the medial superior temporal area of the macaque monkey. *J. Neurophysiol.* 62:642–656.

Tanaka K, Saito H (1989) Analysis of motion of the visual field direction, expansion/contraction, and rotation cells clustered in the dorsal part of the medial superior temporal area of the macaque monkey. *J. Neurophysiol.* 62:626–641.

Traub RD, Jefferys JGR, Miles R (1993) Analysis of the propagation of disinhibition-induced after-discharges along the guinea-pig hippocampal slice in vitro. *J. Physiol. (Lond.)* 472:267–287.

Tsodyks MV, Skaggs EW, Sejnowski TJ, McNaughton BL (1995) Population dynamics and theta rythm phase precession of hippocampal place cell firing: A spiking neuron model. In preparation.

Tsodyks M, Sejnowski TJ (1995) Associative memory and hippocampal place cells. *Int. J. Neural Sys.* 7 (Supp.).

Tsumoto T, Eckart W, Creutzfeldt OD (1979) Modification of orientation selectivity of cat visual cortex neurons by removal of GABA mediated inhibition. *Exp. Brain Res.* 34:351–363.

Usher M, Stemmler M, Koch C, Olami Z (1994) Network amplification of local fluctuations causes high spike rate variability, fractal firing patterns and oscillatory local field potentials. *Neural Comp.* 6:795–836.

Van Vreeswijk C, Abbott LF, Ermentrout GB (1995) Inhibition, not excitation synchronizes coupled neurons. *J. Comp. Neurosci.* 1:313–321.

Vidyasagar TR, Pei X, Volgushev M (1996) Multiple mechanisms underlying the orientation selectivity of visual cortical neurones. *Trends Neurosci.* 19:272–277.

Wadman WJ, Gutnick MJ (1993) Non-uniform propagation of epileptiform discharge in brain slices of rat neocortex. *Neuroscience* 52:255–262.

Wiesel TN, Gilbert CD (1989) Neural mechanisms of visual perception. In D Lam Man-Kit, CD Gilbert, Houston, eds. Neural Mechanisms of Visual Perception, Gulf Publishing Company 2:7–33.

Williams TL, Sigvardt KA, Koppell N, Ermentrout GB, Remler MP (1990) Forcing of coupled nonlinear oscillators: Studies of intersegmental coordination in the lamprey locomotor central pattern generator. *J. Neurophysiol.* 64:862–871.

Wilson HR, Cowan JD (1972) Excitatory and inhibitory interactions in localized populations of model neurons. *Biophys. J.* 12:1–24.

Wörgötter F, Koch C (1991) A detailed model of the primary visual pathway in the cat: Comparison of afferent excitatory and intracortical inhibitory connection schemes for orientation selectivity. *J. Neurosci.* 11:1959–1979.